

(NASA-CR-197608) SHOCK-INDUCED  
DEVOLATIZATION OF CALCIUM SULFATE  
AND IMPLICATIONS FOR K-T  
EXTINCTIONS (California Inst. of  
Tech.) 30 p

N95-19033

Unclass

G3/45 0038408

P16  
PBB-NASA

IN-45-CR

38408

P. 30

## Shock-induced devolatilization of calcium sulfate and implications for K-T extinctions

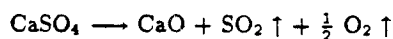
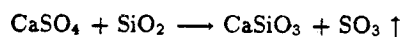
Guangqing Chen, James A. Tyburczy\*, Thomas J. Ahrens†

*Lindhurst Laboratory of Experimental Geophysics, Seismological Laboratory,*

*California Institute of Technology, Pasadena, CA 91125*

November 22, 1993

Calcium sulfate devolatilization during the impact at Chicxulub, Mexico and dispersal in the stratosphere of the resultant sulfuric acid aerosol have been suggested as a possible mechanism for the Cretaceous-Tertiary extinctions [1, 2]. In this paper, we investigated two shock-induced devolatilization reactions of calcium sulfate up to 42 GPa in the laboratory:



We found both to proceed to a much less extent than calculated by equilibrium thermodynamic calculations. Reaction products are found to be  $10^{-2}$  times those calculated for equilibrium. Consequently our estimate of the amount of sulfur oxides degassed into the atmosphere from shock devolatilization of  $\text{CaSO}_4$  in the Chicxulub lithographic section ( $6 \times 10^{15}$ – $2 \times 10^{16}$  g in sulfur mass) is lower by a factor of 70 to 400 than previous estimates, the related environmental stress arising from the resultant global cooling of  $\sim 4$  K and fallout of acid rain does not appear to suffice to explain the widespread K-T extinctions.

\*Also at Department of Geology, Arizona State University, Tempe, AZ 85287

†Correspondent

## 1. Introduction

Since Alvarez *et al.*[3] proposed the Cretaceous-Tertiary (K-T) impact hypothesis, the Chicxulub impact structure has been recognized as the leading candidate for the crater(s) associated with the bolide. Strong supporting evidences relating the Chicxulub, Yucatan crater with the world-wide extinction include the following:

1. Tektites, presumably representing fused target material, from Beloc, Haiti and Mimbral, Mexico K-T sections show the glass source terrane is likely to be a continental margin [4, 5]. This environment contains sediments rich in carbonate and sulfate, which is consistent with Chicxulub stratigraphy. Oxygen and strontium isotope analyses [6] also favor Chicxulub over the Manson, Iowa crater as the source for the tektite-like glassy ejecta, which, in most world-wide locations, has been weathered to various clays;
2. The tektites and Chicxulub melt rock have been ( $^{39}\text{Ar}/^{40}\text{Ar}$ )-dated and found to be coeval within 0.1 m.y. at 65 m.y.[7];
3. Tsunami deposits exactly at K-T boundary, which have now been recognized to occur around the present the Gulf of Mexico. This supports the hypothesis of a nearby impact site[8, 9].

The dominance of calcium carbonate (calcite) and calcium sulfate minerals (anhydrite and gypsum) in the upper 3 km of the Chicxulub section (in the sequence of limestone, anhydrite-dolomite conglomerates, limestone-dolomite and anhydrite-gypsum layers [10]) has led to active research into the effect of their devolatilization upon impact. Previous shock recovery experiments conducted on single crystal calcite found calcite devolatilization upon release to ambient pressure from shock pressures greater than  $\sim 10$  GPa. These experiments have suggested that a Chicxulub-size crater may be capable of increasing the  $\text{CO}_2$  budget of the atmosphere by  $5 \times 10^{18}$  to  $2 \times 10^{19}$  g, therefore the global atmospheric inventory of  $\text{CO}_2$  ( $2.2 \times 10^{18}$  g in pre-industrial age [2],  $2.7 \times 10^{18}$  g at present [11]) could have been increased by a factor of 2 to 10. This is hypothesized to have caused global warming of 2 to 10 K for periods of  $10^4$  to  $10^5$  years [11]. An environmental stress, which affected the proliferation of the wide range of genera which became extinct at the K-T boundary has been suggested to have been induced by impact-liberated  $\text{SO}_2$  or  $\text{SO}_3$  from sulfates. Estimates of the amount of  $\text{SO}_2$  and  $\text{SO}_3$  devolatilization (based on equilibrium conditions)

ranges from  $4 \times 10^{17}$  to  $8 \times 10^{18}$  g. If this amount of sulfur oxides produced stratosphere  $\text{H}_2\text{SO}_4$  aerosol, a rapid temperature decline of 10 to 20 K is predicted to have occurred for several years [1, 2]. In this paper, we present results of calcium sulfate devolatilization experiments under shock conditions via two reactions:



Reaction (A) is of interest because of its lower incipient reaction temperature than reaction (B) (1200 K vs. 1450 K) based on Gibbs formation energy calculations using thermodynamic data in [12] (we assume ambient  $\text{SO}_2/\text{SO}_3$  and  $\text{O}_2$  partial pressures of  $10^{-4}$  and 0.2 bar respectively as in the contemporary atmosphere). Heating experiments carried out in platinum tubes at 1 atm and 1,047–1,406°C suggest this material could be the origin of the yellow Haiti glass[4]. The basement of Chicxulub is generally thought to provide quartz for the reaction, but it is not clear at present how anhydrite/gypsum at shallower depths could have reacted with the basement rocks. Nonetheless, the two reactions have been investigated with anhydrite/silica powder mixture and anhydrite/gypsum polycrystalline disks.

Comparing to theoretical calculations, we found the experimental degree of sulfate devolatilization for powdered samples (particle size was tens of microns) was  $\sim 10^2$  times lower than theoretically estimated. Also, we estimate the mass of sulfur oxides released during the formation of the Chicxulub crater using the upper limit of experimental reaction efficiency. Moreover, upon calculating the anisotropic shock pressure decay in the lithologic rock section in which the Chicxulub crater formed, we estimate is that  $6 \times 10^{15}$  to  $2 \times 10^{16}$  g of sulfur in various oxides could have been generated. Finally, we discuss the possible environmental effects of injecting this amount of sulfur in the form of sulfuric acid and oxides into the stratosphere.

## 2. Recovery experiments

Solid recovery experiments were performed on the Caltech 20 mm and 40 mm propellant guns. Samples ( $\sim 6$  mm in diameter and  $\sim 2$ – $3$  mm in thickness) were encased in stainless steel containers, which were pumped to  $\sim 30$  millitorr vacuum before the shots [13, 14].

### 2.1. Reaction between silica and anhydrite

Experimental parameters are listed in Table 1 (two shock experiments on anhydrite/SiO are listed and will be discussed later). The starting material was a mixture of silica (crystalline or amorphous, Alfa #13024 and 89709) and natural crystalline anhydrite (Ward's Geology #46E0535) powders and was pressed into target container to initial densities of 60–85% of its Archimedian density. Average silica grain size was 4  $\mu\text{m}$ , and anhydrite grains were mostly between 30–100  $\mu\text{m}$ . Equation-of-state constants for the mixture (see Table 2) were calculated from previous anhydrite data of Simakov *et al.*[15] and quartz data of Swegle *et al.*[16] using the formulae by Boslough [17]: assuming uniform stress distribution, for a two-component system,

$$V = m_1 V_1 + m_2 V_2, \quad (1)$$

$$K_{0S} = [(v_1/K_{0S1}) + (v_2/K_{0S2})]^{-1}, \quad (2)$$

$$K'_{0S} = K_{0S}^2 [v_1(1 + K'_{0S1})/K_{0S1}^2 + v_2(1 + K'_{0S2})/K_{0S2}^2] - 1, \quad (3)$$

where  $m_i$ ,  $V_i$ ,  $v_i$ ,  $K_{0Si}$  and  $K'_{0Si}$  are the components' mass fractions, specific volumes, initial volume fractions, bulk moduli and their pressure derivatives at zero pressure. Shock pressures determined by impedance-match method range from 27.4 to 42.3 GPa. Five 20 mm shots and the two 40 mm shots (see Table 1) all had 1:1 molar ratio of anhydrite : silica. The initial porosity of the mixture were 17.2% (1106) to 40.0% (1108); Shot 1107 employed fused quartz; The 40 mm shots were conducted to determine the shock duration effect on the reaction, but no reaction was seen in shot 917, and shot 923 was not recovered; Finally, shots 1109 and 1110 had anhydrite : silica molar ratios of 1:3.7 and 3.0:1. Recovered samples were analyzed with petrographic microscopy, scanning electron microscopy (SEM, instrument: Camscan Series 2 with Tracor Northern EDS detector TH-3/54-6901, operated at 15 kV) and X-ray diffraction (XRD, instrument: Scintag DMC-008, radiation source: Cu-K $\alpha_1$ ). Compared with the original material, the changes exhibited in the 20 mm (except shot 1111, which will be described separately in the following paragraph) post-shock samples are quite similar: in agreement with previous research [18], silica becomes amorphous in spite of its original crystallinity (see XRD spectra in Figure 2); Anhydrite is recovered as a crystalline phase. Although shock-induced mosaicism in the crystal grains was observed with cross-polarized light on petrographic microscope, it appears unlikely that anhydrite

recrystallized from a melt as no rounding of the grains was observed (see Figure 1 a).

In shot 1111 (in which 10 mass% iron powder was intentionally mixed in addition to anhydrite/quartz), devolatilization was much more extensive than the rest of the shots and reaction of iron to iron sulfate and iron sulfide were observed. In their study of sulfur speciation in basaltic glasses [19], Carroll and Rutherford reported that proportion of dissolved sulfur present as sulfate (as opposed to sulfide) increases from near 0% at FMQ (fayalite-magnetite-quartz) oxygen fugacity to near 100% at 2 to 3  $\log f_{O_2}$  units above FMQ. The oxygen fugacity present in these recovery experiments was well into the sulfate stable regime. The presence of iron sulfide led us to believe the greater degree devolatilization of  $CaSO_4$  within 1 mm of the stainless steel container in all the 20 mm shots was affected by the reducing effect of the metal and would not have occurred in its absence. In the central metal-free region, the dimensions of possible reaction zones are so limited that they were nearly at the limit of spatial resolution of the SEM. In the following three sections we will attempt to derive the actual degree of devolatilization from experimentally observed chemical compositions at different locations in the samples.

### 2.1.1. SEM instrument resolution

The SEM electron beam spot is much less than  $1\mu\text{m}$ , but the dimension of excitation volume in the sample, and therefore the instrument resolution, is larger due to electron scattering and secondary fluorescence in the sample [20]. A “smearing” function is assumed to convolve with the “true” chemical composition to give the observed composition. The function form is taken to be Gaussian:

$$f(x) = \frac{1}{\sqrt{\pi}l} e^{-x^2/l^2}, \quad (4)$$

$$\int_{-\infty}^{\infty} f(x) dx = 1 \quad (5)$$

where  $2l$  is a measure of spatial resolution. Anhydrite and quartz disks of  $\sim 1$  mm thickness each were sandwiched together and heated at 573 K for 6 hours, followed by a 24-hour press at  $\sim 4000$  psi so that plastic flow may take place to produce a good contact (with less-than- $1\mu\text{m}$  gap) as a no-reaction reference. A comparison between the SEM analysis across the pressed boundary and calculation (convolution of Equation 4 and a step function) found  $l = 0.53\mu\text{m}$  to provide the best fit (Figure 3). This agrees with our expectation that the resolution distance is larger than the electron beam diameter.

The data in Figures 3 and 4 are corrected for secondary fluorescence excited by characteristic radiations. Another concern has been the fluorescence excited by the continuous spectrum. We use an approximate equation ((15.10) in Reed [21]), modified for compounds by multiplying the ratio of mass attenuation coefficients of the excited element  $A$  ( $\mu_C^A$ ) and the compound ( $\mu_C$ ), the intensity of fluorescence  $I_f$  relative to electron-excited characteristic K-radiation of element  $A$  in the compound  $I_C^A$  is thus

$$\frac{I_f}{I_C^A} = 9.7 \times 10^{-8} Z^4 \frac{\mu_C^A}{\mu_C}, \quad (6)$$

( $Z$  is the atomic number of the excited element). The correction factor for continuum fluorescence is

$$F_f = 1 / (1 + \frac{I_f}{I_C^A}). \quad (7)$$

We consider three cases:

1. Compound is 50 mol.%  $\text{CaSO}_4$  and 50 mol.%  $\text{SiO}_2$  (in the middle of the mixing zone),  
 $I_f^{\text{Ca}}/I_C^{\text{Ca}}=1.21\%$ ,  $I_f^{\text{S}}/I_C^{\text{S}}=0.24\%$ ;
2. Compound is near 100%  $\text{SiO}_2$  with a trace of Ca and S (deep into silica).  $I_f^{\text{Ca}}/I_C^{\text{Ca}}=0.67\%$ ,  
 $I_f^{\text{S}}/I_C^{\text{S}}=0.13\%$ ;
3. A sharp  $\text{CaSO}_4$ - $\text{SiO}_2$  boundary, with the electron beam shifted to  $\text{SiO}_2$  side so that the electron-excitation volume is completely in  $\text{SiO}_2$ . Any Ca and S signal is purely due to secondary fluorescence from the  $\text{SiO}_2$  continuum (Si characteristic line is not energetic enough to excite Ca or S). The secondary fluorescence intensity, relative to electron-excited radiation in pure  $\text{CaSO}_4$ , is given by:

$$\frac{I_f^{\text{Ca,S}}}{I_{\text{CaSO}_4}^{\text{Ca,S}}} = 0.5 \times 9.7 \times 10^{-8} Z^4 \frac{\mu_{\text{CaSO}_4}^{\text{Ca,S}}}{\mu_{\text{CaSO}_4}}. \quad (8)$$

Equation 8 is very similar to Equation 6 except the factor 0.5, which arises because only half of the continuous radiation goes into  $\text{CaSO}_4$ , neglecting the finite width of the primary X-ray source. The ratios for Ca and S calculated are 0.23% and 0.11%.

More detailed numerical calculations were done and the results agree within  $\pm 0.3\%$ . Case (3) agrees very well with observations at  $1 \mu\text{m}$  in quartz from the cold-pressed boundary, where Ca and S signal intensities are  $0.2 \pm 0.1\%$  and  $0.4 \pm 1\%$  of those in pure  $\text{CaSO}_4$  (Figure 3). For the shock-recovered samples, the Ca

and S intensities within  $\sim 3\mu\text{m}$  from the boundaries are much higher than the secondary fluorescence level and the corrections are negligible compared to the analytical uncertainty.

### 2.1.2. *Mixing of sulfate with silica*

In shocked samples the boundary layer between calcium sulfate and silica is thicker than the cold-pressed edge. In the following we examine several possible mixing mechanisms:

#### 1. Solid state diffusion:

The diffusion constants of H,  $^{18}\text{O}$  and  $^{30}\text{Si}$  atoms in quartz have been documented in [22]. At  $800^\circ\text{C}$ , they vary over a wide range, with H having the highest  $D = 2.5 \times 10^{-11} \text{ m}^2/\text{s}$ , and  $^{30}\text{Si}$  having the lowest  $D = 1.3 \times 10^{-21} \text{ m}^2/\text{s}$ . In the time scale of our experiments  $\sim 1\mu\text{s}$ , the characteristic distance  $\sqrt{Dt} \sim 10^{-8}-10^{-2}\mu\text{m}$  is much smaller than the observed reaction zone thickness;

#### 2. Liquid state diffusion:

Rubie *et al.* directly measured oxygen self-diffusivity in  $\text{Na}_2\text{Si}_4\text{O}_9$  melt up to  $1825^\circ\text{C}$  and between 4–10 GPa [23]. The diffusion constant they reported ranges from 1.0 to  $4.2 \times 10^{-10} \text{ m}^2/\text{s}$  increasing with temperature and pressure. Si-O bond breaking is the basic process controlling both O self-diffusion in  $\text{Na}_2\text{Si}_4\text{O}_9$  and  $\text{CaSO}_4$  diffusion in silica melt which is of present interest. It is possible to use these data to obtain an order-of-magnitude estimate of mixing time and length scales in the  $\text{SiO}_2$  liquid. Again, in the  $1\mu\text{s}$  shock duration, the highest diffusivity ( $4.20 \times 10^{-10} \text{ m}^2/\text{s}$ ) gives characteristic distance  $2 \times 10^{-2}\mu\text{m}$ , which is still too small to account for the  $\mu\text{m}$ -size mixing layer;

#### 3. Rayleigh-Taylor instability:

Although initially crystalline quartz is amorphized during shock, we cannot conclude that it has been once molten because quartz can transform to diaplectic glass without melting [18]. Since there is a strong contrast in strength of quartz and anhydrite ( $\sim 1 \text{ GPa}$  for quartz and  $\sim 0.1 \text{ GPa}$  for anhydrite), we suggest Rayleigh-Taylor instability as the third mixing mechanism.

Rayleigh-Taylor instability arises at interfaces between two materials of different strength when they are strongly accelerated or decelerated along a direction perpendicular to their planar interface. According to the theoretical model by Drucker[24], when shock wave propagates from the stronger

material into the weaker material, the interface experiences alternating compressional and tensile stress due to perturbations (bumps) on material surface. When the stress difference exceeds the strength of the stronger material ( $\sigma_0$ ), the bumps grow freely and instability occurs. Two important derivations of the theory are threshold perturbation amplitude:

$$h_0^{th} = H(1 + \pi/2)\sigma_0 F/P, \quad (9)$$

and time dependence of instability growth above the threshold:

$$h - h_0^{th} = (h_0 - h_0^{th}) \cosh \sqrt{\beta Pt/(\lambda \rho H)}, \quad (10)$$

where  $H$  is material thickness,  $h_0$  is initial perturbation amplitude,  $\rho$  is material density,  $P$  is shock pressure,  $\lambda$  is the perturbation wavelength,  $F$  is a geometric factor between 0.25-1, and  $\beta = \frac{16}{(4+\pi)F} \sim 2-8$ .

A prominent feature of the theory is that the threshold is independent of wavelength  $\lambda$ . Experiments by Barnes *et al.* on aluminum and 304 stainless steel plates support the theoretical prediction [25]. For our case,  $\sigma_0 \sim 1$  GPa,  $\rho=2.65$  g/cm<sup>3</sup>,  $P=40$  GPa,  $\lambda \sim H \sim$  grain size  $4\mu\text{m}$ , the threshold thickness perturbation calculated from Equation 9 is  $\sim 0.4\mu\text{m}$ , which is very reasonable. Above threshold, the growth is very fast: for an initial perturbation 10% above threshold, Equation 10 indicates that it takes a few nanoseconds to grow to sizes comparable to  $\lambda/2$ , after which the theory is no longer valid.

From the above discussion, only Rayleigh-Taylor instability emerges as a plausible mixing mechanism. Although it is not a diffusive process, we describe the shocked sample interface mathematically by a linear diffusion profile. Denote  $g_{Ca}(x)$  = the molar ratio of Ca/O, the solution of one dimensional diffusion equation (heat equation, see, *e.g.*, [26]) with initial conditions:

$$g_{Ca}(x)|_{t=0} = \begin{cases} 0.25 & \text{if } x \leq 0 \\ 0 & \text{if } x > 0 \end{cases}$$

is

$$g_{Ca}(x) = \frac{1}{8} \text{erfc}(x/L). \quad (11)$$

A fit to the shocked sample profile (convolved with  $f(x)$ ) gives the mixing length  $L \simeq 1.5\mu\text{m}$  (solid line in Figure 3):

$$g_{Ca}^{SEM}(x) = \int_{-\infty}^{\infty} f(x-x')g_{Ca}(x')dx' \quad (12)$$

### 2.1.3. Degree of devolatilization

The experimentally seen devolatilization shows some scatter (Figure 4). For simplicity, we assume an average of 20% S molar loss in the region  $-L < x < L$ , so the ratio S/O is

$$g_S(x) = 0.8g_{Ca}(x) = 0.1\text{erfc}(x/L). \quad (13)$$

The S/Ca profile observed on SEM is given by

$$(S/Ca)(x) = \frac{\int_{-\infty}^{\infty} g_S(x')e^{-(x'-x)^2/l^2} dx'}{\int_{-\infty}^{\infty} g_{Ca}(x')e^{-(x'-x)^2/l^2} dx'} \quad (14)$$

Bulk devolatilization, defined as the fraction of sulfur loss in the boundary layer over the total sulfur mass in the original sample, is given by

$$DV = \frac{3 \times \int_{-L}^L (g_{Ca} - g_S) dx}{g_{Ca}|_{x=-\infty} R}, \quad (15)$$

where  $R$  is the anhydrite grain size. The factor 3 takes into account the three dimensional effect. For  $R = 100\mu\text{m}$ , evaluation of the formula yields a numerical value of  $DV = 6 \times 10^{-3}$ .

We infer that anhydrite mixed into silica upon shock loading and underwent devolatilization during release. Tyburczy and Ahrens [13] used the following approach to calculate the extent of shock-induced reactions:

1. Entropy excess required for incipient reaction:

$$S_{IR} = \int_{T_0}^{T_{IR}} \frac{C_p}{T} dT, \quad (16)$$

where  $T_0$  is room temperature,  $T_{IR}$  is the temperature of incipient reaction (at which the sums of Gibbs formation energies for the reactants and products are equal),  $C_p$  is the atmospheric pressure heat capacity at constant pressure.

2. Entropy excess required for complete reaction:

$$S_{CR} = S_{IR} + \Delta S - \sum_{\text{gas products}} n_i R \ln(P_i/P_0), \quad (17)$$

where  $\Delta S$  is the entropy difference between reactants and products as computed from Robie *et al.* [12], the last term on the right takes into account effects of partial pressures,  $P_i$ , of gas products ( $P_0$  is the ambient pressure),  $n_i$  is the number of moles of gas specie  $i$ ,  $R$  is the gas constant (8.31 J mol<sup>-1</sup>K<sup>-1</sup>).

3. Entropy gain in the shocked state (and in the post-shock state assuming isentropic release):

$$\Delta S_H = S_{tr} + C_v \ln(T_H/T_S), \quad (18)$$

where  $S_{tr}$  is the entropy change of phase transition during compression,  $T_S$  is the temperature of isentropic compression from initial volume  $V_0$  at temperature  $T_i$  to Hugoniot volume  $V_H$  and isentropic pressure  $P_s$ :

$$T_s = T_i \exp \left[ - \int_{V_0}^{V_H} \left( \frac{\gamma}{V} \right) dV \right] \quad (19)$$

where  $\gamma$  is the Grüneisen parameter.  $T_H$  is the shock temperature, determined by:

$$\frac{V_H}{\gamma} (P_H - P_s) = \int_{T_i}^{T_H} C_v dT \quad (20)$$

$C_v$  is heat capacity at constant volume (at high pressure).

4. The extent of reaction is given by:

$$\text{Fraction of material reacted} = \frac{\Delta S_H - S_{IR}}{S_{CR} - S_{IR}}. \quad (21)$$

The results from Equation 21 for reactions (A) and (B) are shown as the solid and broken curves in Figure 5. The equation-of-state parameters are the same as in Table 2, and  $S_{tr}=0$  for the calculation. Local devolatilization in the reaction layer is close to theoretical calculation, but decomposed anhydrite is only a small portion ( $\sim 6 \times 10^{-3}$ ) of the total mass because of the dimension of the reaction layer is much smaller relative to the grain size ( $\sim 100 \mu\text{m}$ ). In the Chicxulub section, mixing of calcium sulfate and quartz was certainly less intimate, the reaction efficiency should be even lower.

## 2.2. Decomposition of anhydrite and gypsum alone

Since calcium sulfate strata often do not occur close to quartz in the Chicxulub section, decomposition of anhydrite/gypsum is an important issue to the evaluation of sulfur oxides production. Similar recovery

experiments up to 42.7 GPa have been conducted on anhydrite and gypsum samples (Table 3). The samples were nonporous single crystalline gypsum and polycrystalline anhydrite disks approximately 4 mm in diameter and 0.5–1 mm in thickness (mass 20–30 mg). In several of the shots the samples were sandwiched between Zn disks in an attempt to enhance solid recovery.

On SEM images (Figure 1 b), the recovered samples show textures that are not different from unshocked anhydrite and gypsum. There is no indication of inhomogeneous shear band heating which has been recognized as the major volatile loss mechanism for calcite [27]. Thermogravimetric analysis (TGA) was performed on Thermal Analysis System SETARAM TG92. Milligram-mass samples were analyzed in a He atmosphere, heating from 25 to 1600°C at a heating rate of 2°C/min. Impact-induced mass loss was determined as the difference in mass loss between shocked and unshocked samples. TGA and chemical analyses on the SEM (on apparatus described previously) revealed no variation in sulfur concentration beyond analytical uncertainty (~ 2%). Devolatilization of 72–76% of the total H<sub>2</sub>O was detected by TGA in shocked gypsum (Table 3).

In summary, in the pressure range covered by the experiments, the fraction of sulfur, by mass, that degassed is ~ 10<sup>-2</sup> of theoretical prediction (Figure 5), and overall sulfur devolatilization is minimal. Both reactions (A) and (B) are endothermic, with rather large enthalpy increases of 313 (for α-quartz as reactant, 305 for fused quartz) and 502 kJ per mole reacted CaSO<sub>4</sub> [12], which are 17 and 27% of the specific shock energy of a 40 GPa impact on non-porous materials. To examine the role of enthalpy difference in shock-induced reactions, we conducted two recovery experiments on anhydrite and amorphous silicon monoxide (SiO, Alfa #89430) powder mixture (Table 1). The reaction in question is



We observed extensive reaction in the recovered material of shot 1098, where S in anhydrite is reduced by a factor of 4–5. Although enthalpy of SiO glass is unknown, it is a less stable compound than quartz and therefore absorbs less energy in reaction (C). The weaker bonding structure compared to SiO<sub>2</sub> could also give rise to a much higher diffusion rate. Both may contribute to the excessive reaction occurred.

### 3. Implications for the K-T boundary

#### 3.1. Pressure decay in the transient Chicxulub crater

Previous studies on crater formation mechanisms give formulae for pressure decay with distance  $R$  along the centerline in a transient crater [29, 30, 31]. For example, Ahrens and O'Keefe [29] calculated gabbroic anorthosite or iron meteorites cratering planetary anorthosite target and fit their calculations with two branches using exponential functions of the form:

$$\log_{10}(P/\text{Mbar}) = a \log_{10}(R/R_0) + b \quad (22)$$

where  $R_0$  is the radius of the meteorite, parameters  $a$  and  $b$  assume different values for different targets and in the near- and far-field ( $a < 0$ ).

The Schmidt-Holsapple scaling [31] breaks down the pressure decay in large craters into four ranges—near source, strong shock, intermediate shock and material strength regimes, in each of which the peak shock pressure decays exponentially with normalized distance  $R/R_0$ , the exponents (equivalent to parameter  $a$  in Ahrens-O'Keefe model) are 0, -3.6, -1.8 and -1.18 in successive regimes away from impact center.

These two approaches give roughly the same pressure decay profiles if the parameters are chosen properly. A more important effect to take into account in evaluating sulfate devolatilization is the deviation of equi-pressure contours from a hemispherical surface because of rarefaction wave from the target free surface. Define  $V_{\text{actual}}^{\text{vapor}}$  and  $V_{\text{actual}}^{\text{melt}}$  to be the vaporization and melt volumes (normalized to impactor volume) given in O'Keefe and Ahrens [30],  $V_{\text{h.s.}}^{\text{vapor}}$  and  $V_{\text{h.s.}}^{\text{melt}}$  to be the normalized vaporization and melt volumes calculated assuming hemispherical peak shock pressure contours. For a 15 km/s anorthosite meteorite impacting anorthosite  $V_{\text{actual}}^{\text{melt}}/V_{\text{h.s.}}^{\text{melt}}$  is only 0.052; For a 45 km/s anorthosite on anorthosite impact,  $V_{\text{actual}}^{\text{melt}}/V_{\text{h.s.}}^{\text{melt}}=0.040$ ,  $V_{\text{actual}}^{\text{vapor}}/V_{\text{h.s.}}^{\text{vapor}}=0.042$ ; For a 15 km/s iron on anorthosite impact,  $V_{\text{actual}}^{\text{melt}}/V_{\text{h.s.}}^{\text{melt}}=0.426$ . In this paper, we modify the simple model by assigning each hemispherical shell an “average” pressure that is lower than the centerline pressure. Although this is not a rigorous treatment, it can be regarded as a first-order correction for the effect of the two-dimensional rarefaction wave (Figure 6). The pressures of the points labeled “complete vaporization” and “complete melting” are complete phase change pressures, their radii are chosen such that the hemispherical volumes within are

equal to the volumes given in [30]. Such derived  $a, b$  parameters for the “average” pressure attenuation are listed in Table 4.

A few noticeable features in Figure 6:

1. Near impact center, pressure profile is dominated by the initial shock, centerline and average pressures should not differ very much;
2. Their deviation grows larger at larger radius as rarefaction wave becomes important;
3. At great depth (far away from the target surface), self-similarity is established, the average pressure curve is parallel but offset downward to the centerline pressure curve.

In Figure 7, centerline pressure profiles given by Holsapple-Schmidt scaling [31] and Ahrens-O’Keefe formula [29] are plotted together with estimated averaged pressure for transient Chicxulub crater, assumed to behave as gabbroic anorthosite, if the bolide was an chondritic asteroid, also similar in behavior as gabbroic anorthosite. The effect of different initial impact velocity is represented through the center peak pressure. The average pressure decay is then deduced from the Ahrens-O’Keefe profile and the corrections in Table 4. Based on this profile, the theoretical incipient devolatilization pressure ( $\approx 25$  GPa) corresponds to a devolatilization hemispheric diameter of 50 km in the target rocks.

An alternative scenario is the bolide was a comet ( $\rho \approx 1$  g/cm<sup>3</sup>,  $v \approx 60$  km/s). From *in situ* mass spectrum measurements in several Halley flybys by the Giotto and Vega spacecraft in 1986, it was found [32] the element composition of the comet is similar (within a factor of two) relative to CI chondrites for elements heavier than O. The comet is much more enriched in CHON elements, and as a result, the atomic concentrations of heavy elements are about one fourth of the corresponding values for chondrites. Since the average atomic weight is also lower for the comet ( $\approx 9.6$  vs.  $\approx 14.9$  for chondrites), the comet/chondrite mass abundance ratio for heavy elements is about 0.4. To maintain the global Ir anomaly constant (estimated at  $3.7 \times 10^{10}$  g from the Gubbio section [3]), the comet’s diameter has to be around 14 km. Following a similar calculation as for a gabbroic anorthosite asteroid, the devolatilization hemispheric diameter would become 97 km.

### 3.2. Conclusions

Our experiments do not cover the entire pressure range of the K-T impact, but our results show conclusively that shock-induced calcium sulfate devolatilization requires higher shock pressure than devolatilization of serpentine, calcite and Murchison carbonaceous chondrite [13, 27, 33]. The extent of devolatilization reactions are on the order of  $10^{-2}$  less than predicted via equilibrium calculation. One reason for this appears to be the lack of shear bands in anhydrite/gypsum and poor mixing between anhydrite and silica. Scaling up to the Chicxulub crater gives a rough estimate of sulfur degassing during its formation.

Assume:

1. A 500 m-thick calcium sulfate bed 1 km below surface [1] in which 50% of the mass was  $\text{CaSO}_4$ ,
2. the degree of reaction was about 2% (upper limit of experimental uncertainty of anhydrite/gypsum devolatilization) within the reaction diameter,

the total degassed sulfur mass was  $6 \times 10^{15}$  g (in forms of  $\text{SO}_2$  and  $\text{SO}_3$ ) for an asteroid impact. Under the same assumptions, the estimate in case of a comet impact was  $2 \times 10^{16}$  g.

This mass is much less than previous estimates given by Brett [1] or Sigurdsson *et al.* [2] ( $4 \times 10^{17}$ – $8 \times 10^{18}$  g) mainly due to the experimentally observed devolatilization occurs to a much lower extent (by a factor of 70 to 400) than previously assumed, but it is still about one to two orders of magnitude above the amount of  $\text{SO}_2$  released by the eruption of Tambora in 1815 (estimated at  $1$ – $2 \times 10^{14}$  g and caused cooling of 0.7 K in the following 2 years [34, 36, 37]). However, our estimate supports Blum *et al.*'s suggestion that most of the Haiti yellow glass was derived from shock-induced mixing of silicates with carbonates rather than sulfate-bearing rocks [6].

How the reactions proceed at pressures under which the reactants are molten is not answered by our present experiments. To give an upper limit, we assume perfect mixing and 100% devolatilization inside 34 km hemispheric diameter from the center of the Chicxulub crater (which corresponds to pressures greater than 52 GPa), the amount of S released is about  $1.4 \times 10^{17}$  g, which is still a factor of 3 lower than previous estimates. However, we regard such an amount as unlikely.

### 9.3. Environmental effects

The theory of lofting of impact volatized  $\text{SO}_2$  and  $\text{SO}_3$  from a crater and temperature decline due to the increase in optical depth resulting from stratospheric  $\text{H}_2\text{SO}_4$  aerosol has yet to be worked out. Therefore, evaluation of the environment effects of the K-T impact mostly relies on climatic changes after historic large volcanic eruptions. Sigurdsson used the following empirical relation to correlate the volcanic sulfur mass yield  $x$ , in grams, to observed temperature decreases after the eruptions [35]

$$\Delta T = 5.9 \times 10^{-5} x^{0.31} \quad (23)$$

Extrapolating to our estimate of sulfur release ( $x=6 \times 10^{15}$ – $2 \times 10^{16}$ ), it is expected to give rise to short term global cooling of  $\sim 4$ – $6$  K and acid rainout of  $40$ – $150$  g/m<sup>2</sup> on the earth's surface. Recently, Vogelmann *et al.* [38] discussed the effect of volcanic  $\text{SO}_2$  release on the ozone layer by providing  $\text{H}_2\text{SO}_4$  aerosol surfaces on which chlorine can react to forms that catalyze ozone depletion [39, 40]. Vogelmann *et al.* point out that the resulting increase in UV-B radiation (290–320 nm) could be biologically hazardous even for large volcanic eruptions. However,  $\text{H}_2\text{SO}_4$  aerosol also increases optical depth in the UV radiation, which could partially compensate for ozone depletion. The relation between  $\text{SO}_2$  release and ozone depletion is not established at present. In conclusion, we suggest that in a few years after the K-T impact, the volatized sulfur oxides and sulfuric acid aerosol would have caused a drop in the earth's temperature by  $4$ – $6$  K, but the cooling could have been partially or completely offset by the  $\text{CO}_2$  green house effect. As sulfuric acid aerosol separated from the atmosphere, the earth underwent a more persistent warm period of tens of thousands of years when the temperature was raised by as much as  $10$  K [11]. The environmental effects of sulfate devolatilization could have been quite hazardous, but itself alone may not suffice as a potent extinction mechanism.

### Acknowledgments

We thank E. Gelle and M. Long for their help in performing the recovery experiments. Prof. Donald Burnett and Dr. John Armstrong provided valuable discussions on SEM analysis. TGA was performed in the Materials Preparation Facility in the Center for Solid State Science at Arizona State University.

Research supported by NASA. Contribution # 5350, Division of Geological and Planetary Sciences.

## References

- 1 R. Brett, The Cretaceous-Tertiary extinction: A lethal mechanism involving anhydrite target rocks. *Geochim. et Cosmo. Acta*, 56, 3603-3606 (1992).
- 2 H. Sigurdsson, S. D'Hondt and S. Carey, The impact of the Cretaceous/Tertiary bolide on evaporite terrane and generation of major sulfuric-acid aerosol. *Earth and Planetary Sci. Lett.* 109, 543-559 (1992).
- 3 L. W. Alvarez, W. Alvarez, F. Asaro and H. V. Michel, Extraterrestrial cause for the Cretaceous/Tertiary extinction. *Science*, 208, 1095-1108 (1980).
- 4 H. Sigurdsson, Ph. Bonté, L. Turpin, M. Chaussidon, N. Metrich, M. Steinberg, Ph. Prade and S. D'Hondt, Geochemical constraints on source region of Cretaceous/Tertiary impact glasses. *Nature*, 353, 839-842 (1991).
- 5 H. Sigurdsson, S. D'Hondt, M. A. Arthur, T. J. Bralower, J. C. Zachos, M. Fossen and J. E. T. Channell, Glass from the Cretaceous Tertiary boundary in Haiti. *Nature*, 349, 482-487 (1991).
- 6 J. D. Blum and C. P. Chamberlain, Oxygen isotope constraints on the origin of impact glasses from the Cretaceous-Tertiary boundary, *Science*, 257, 1104-1107 (1992).
- 7 C. C. Swisher III, J. M. Grajales-Nishimura, A. Montanari, S. V. Margolis, P. Claeys, W. Alvarez, P. Renne, E. Cedillo-Pardo, F. J.-M. R. Maurrasse, G. H. Curtis, J. Smit and M. O. McWilliams, Coeval Ar-40/Ar-39 ages of 65.0 million years ago from Chicxulub crater melt rock and Cretaceous-Tertiary boundary tektites, *Science*, 257, 954-958 (1992).
- 8 J. Bourgeois, T. A. Hansen, P. L. Wiberg and E. G. Kauffman, A tsunami deposit at the Cretaceous-Tertiary boundary in Texas, *Science*, 241, 567-570 (1988).
- 9 J. Smit, A. Montanari, N. H. M. Swinburne, W. Alvarez and A. R. Hildebrand, Tektite-bearing, deep-water clastic unit at the Cretaceous-Tertiary boundary in northeastern Mexico, *Geology*, 20, 99-103 (1992).
- 10 C. Koeberl, Chicxulub crater, Yucatan-tektites, impact glasses, and the geochemistry of target rocks and breccias, *Geology*, 21, 211-214 (1993).
- 11 J. D. O'Keefe and T. J. Ahrens, Impact production of CO<sub>2</sub> by the Cretaceous/Tertiary extinction bolide and the resultant heating of the Earth, *Nature*, 338, 247-249 (1989).
- 12 R. A. Robie, B. S. Hemingway and J. R. Fisher, Thermodynamic Properties of Minerals and Related Substances at 298.15K and 1 Bar (10<sup>5</sup> Pascals) Pressure and at Higher Temperatures. *U. S. Geol. Survey Bull.* 1452 (1979).

- 13 J. A. Tyburczy and T. J. Ahrens, Dynamic compression and volatile release of carbonates. *J. Geophys. Res.*, 91, 4730-4744 (1986).
- 14 M. A. Lange, P. Lambert and T. J. Ahrens, Shock effects on hydrous minerals and implications for carbonaceous meteorites. *Geochim. Cosmochim. Acta*, 49, 1715-1726 (1985).
- 15 G. V. M. N. Simakov, N. M. Pavlovskiy, N. G. Kalashnikov and R. F. Trunin, Shock compressibility of twelve minerals. *Izv. Phys. Solid Earth* 8, 488-492 (1974).
- 16 J. W. Swegle, Irreversible phase-transitions and wave-propagation in silicate geologic materials. *J. Appl. Phys.*, 68, 1563-1579 (1990).
- 17 M. B. Boslough, A thermochemical model for shock-induced reactions (heat detonations) in solids. *J. Chem. Phys.* 92, 1839-1848 (1990).
- 18 F. Hörz, Statistical measurements of deformation structures and refractive indices in experimentally shock loaded quartz. *Shock metamorphism of natural materials*, B. M. French and N. M. Short (eds.), Mono Book Corp., Baltimore, 243-254 (1968).
- 19 M. R. Carroll and M. J. Rutherford, Sulfur speciation in hydrous experimental glasses of varying oxidation state: Results from measured wavelength shifts of sulfur X-rays, *Am. Mineralogist*, V 73, 845-849 (1988).
- 20 J. I. Goldstein, D. E. Newbury, P. Echlin, D. C. Joy, A. D. Romig, Jr., C. E. Lyman, C. Fiori and E. Lifshin, *Scanning electron microscopy and X-ray microanalysis: a text for biologists, materials scientists, and geologists*, 2nd edition, Plenum Press, New York (1992).
- 21 S. J. B. Reed, *Electron microprobe analysis*, Cambridge University Press (1975).
- 22 J. B. Brady, Diffusion Data for Silicate Minerals, Glasses, and Liquids, in *Handbook of Physical Constants*, ed. by T. J. Ahrens, Am. Geophys. U. *in print*.
- 23 D. C. Rubie, C. R. Ross II, M. R. Carroll and S. C. Elphick, Oxygen self-diffusion in  $\text{Na}_2\text{Si}_4\text{O}_9$  liquid up to 10 GPa and estimation of high-pressure melt viscosities, *Am. Mineralogist*, V 78, 574-582 (1993).
- 24 D. C. Drucker, "Taylor Instability" of the Surface of an Elastic-Plastic Plate, *Mechanics Today*, V 5, Pergamon Press, New York (1975).
- 25 J. F. Barnes, D. H. Janney, R. K. London, K. A. Meyer, D. H. Sharp, Further Experimentation on Taylor Instability in Solids, *J. Appl. Phys.* 51, 4678-4679 (1980).
- 26 P. W. Berg and J. L. McGregor, *Elementary Partial Differential Equations*, Holden-Day, San Francisco (1966).

- 27 M. A. Lange and T. J. Ahrens, Shock-induced CO<sub>2</sub> loss from CaCO<sub>3</sub>; implications for early planetary atmospheres. *Earth and Planetary Sci. Lett.* 77, 409-418 (1986).
- 28 S. P. Marsh, *LASL Shock Hugoniot Data*, University of California Press, Berkeley (1980).
- 29 T. J. Ahrens and J. D. O'Keefe, Equation of state and impact-induced shock-wave attenuation on the moon, in *Impact and Explosion Cratering*, ed. by D. J. Roddy, R. O. Pepin, R. B. Merrill, Pergamon Press, New York, 639-656 (1977).
- 30 J. D. O'Keefe and T. J. Ahrens, Impact-induced energy partitioning, melting, and vaporization on terrestrial planets, *Proc. Lunar Sci. Conf. 8th*, 3357-3374 (1977).
- 31 K. Holsapple, The scaling of impact processes in planetary sciences, *Ann. Rev. of Earth and Planet. Sci.* 21, 333-373 (1993).
- 32 E. K. Jessberger, J. Kissel and J. Rahe, The composition of comets, in *Origin and Evolution of Planetary and Satellite Atmospheres*, ed. by S. K. Atreya, J. B. Pollack, M. S. Matthews, University of Arizona Press, Tucson (1989).
- 33 J. A. Tyburczy, B. Frisch and T. J. Ahrens, Shock-induced volatile loss from a carbonaceous chondrite - implications for planetary accretion, *Earth and Planetary Sci. Lett.* 80, 201-207 (1986).
- 34 J. P. Pinto, R. P. Turco and O. B. Toon, Self-limiting physical and chemical effects in volcanic eruption clouds. *J. Geophys. Res.*, 94, 11165-11174 (1989).
- 35 H. Sigurdsson, Assessment of the atmospheric impact of volcanic eruptions, in *Global Catastrophes in Earth History; An Interdisciplinary Conference on Impact, Volcanism, and Mass Mortality*, ed. by V. L. Sharpton, P. D. Ward and T. B. Museum, *Geol. Soc. Am., Spec. Pap.* 247, 99-110 (1990).
- 36 H. Sigurdsson, Evidence of volcanic loading of the atmosphere and climate response. *Palaeogeog. Palaeoclim. Palaeoeco.* 89, 277-289 (1990).
- 37 D. M. Pyle, On the climatic effectiveness of volcanic-eruptions, *Quaternary Research*, 37, 125-129 (1992).
- 38 A. M. Vogelmann, T. P. Ackerman and R. P. Turco, Enhancements in biologically effective ultraviolet-radiation following volcanic-eruptions, *Nature*, 359, 47-49 (1992).
- 39 D. J. Hofmann, S. Solomon, Ozone destruction through heterogeneous chemistry following the eruption of el chichon, *J. Geophys. Res.*, 94, 5029-5041 (1989).
- 40 R. P. Turco, P. Hamill, Supercooled sulfuric-acid droplets - perturbed stratospheric chemistry in early winter, *Ber. Bunsenges. Phys. Chem.*, 96, 323-334 (1992).

## Tables

TABLE 1. Recovery experiments on anhydrite/silica and anhydrite/SiO.

Shot # <sup>1</sup>	Sample	Molar ratio (anhydrite:silica)	Projectile	$V_{proj}$ (km/s)	$P_{peak}$ (GPa)
1106	anhydrite/qtz	1:1	Ta	1.87	33.8
1107	anhydrite/fused qtz	1:1	W	2.02	42.2
1108	anhydrite/qtz	1:1	Ta	1.92	35.0
1109	anhydrite/qtz	1:3.7	Ta	1.90(?)	42.3
1110	anhydrite/qtz	3.0:1	Ta	1.94	32.5
1111	anhydrite/qtz/Fe	1:1	Ta	1.89	34.3
1112	anhydrite/qtz	1:1	Ta	1.88	34.1
917(40mm gun)	anhydrite/qtz	1:1	Ta	1.59	27.4
923(40mm gun)	anhydrite/qtz	1:1	Ta	1.77	31.5
1098	anhydrite/SiO	—	W	2.06	—
1099	anhydrite/SiO	—	Ta	1.58	—

<sup>1</sup> On Caltech's 20mm gun unless noted otherwise.

TABLE 2. Equation-of-state constants of  
anhydrite, silica and their mixture.

Material	$\rho$ (g/cm <sup>3</sup> )	$K_{OS}$ (GPa)	$K'_{OS}$
Anhydrite (LPP)	2.97	38.5	6.0
Silica (HPP)	4.29	350	3.3
Mixture (1:1 molar)	3.28	48.7	7.6

TABLE 3. Recovery experiments on anhydrite and gypsum.

Shot # <sup>1</sup>	Sample	Projectile	$V_{\text{proj}}$ (km/s)	$P_{\text{peak}}$ (GPa) <sup>2</sup>	H <sub>2</sub> O loss (%)
1090	anhydrite	Ta	1.11	23.6	—
1091	anhydrite	Ta	1.48	33.2	—
1092	anhydrite	Ta	1.66	38.0	—
1103	anhydrite	Ta	1.77	41.2	—
1093	anhydrite	Ta	1.82	42.7	—
1101	gypsum	Ta	1.35	29.7	72
1094	gypsum	Ta	1.59	36.2	76
1102	gypsum	Ta	1.81	42.1	76

<sup>1</sup> On Caltech's 20mm gun.

<sup>2</sup> Calculated using stainless steel equation of state [28].

TABLE 4. Centerline and average pressure attenuation:  
 $\log_{10}(P/\text{Mbar}) = a \log_{10}(R/R_0) + b$

		Near-field		Far-field	
		a	b	a	b
An→An	Centerline <sup>1</sup>	-0.293	1.208	-2.15	2.373
45 km/s	Average	-0.616	0.947	-2.18	1.394
An→An	Centerline <sup>1</sup>	-0.222	0.285	-1.97	1.399
15 km/s	Average	-0.608	-0.024	-1.97	0.556
Fe→An	Centerline <sup>1</sup>	-0.295	0.470	-2.49	1.475
15 km/s	Average			-2.49	1.167

<sup>1</sup>After Ahrens and O'Keefe [29].

TABLE 5. Parameters  $a, b$  used to estimate peak and average pressures of Chicxulub crater.

	Near-field		Far-field	
	$a$	$b$	$a$	$b$
Centerline	-0.222	0.501	-1.97	1.62
Average	-0.608	0.192	-1.97	0.772

## Figures

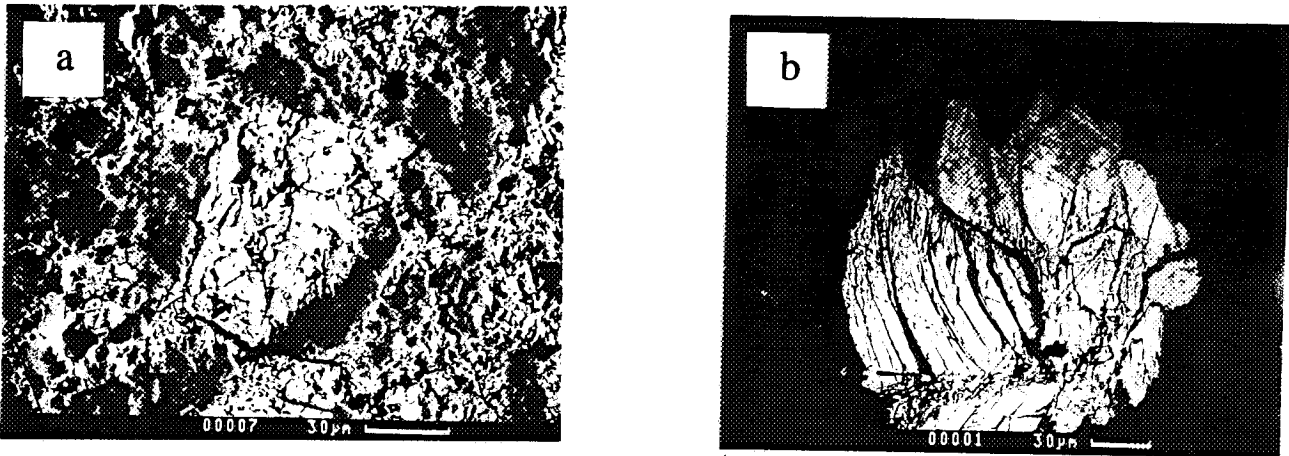


Fig. 1. SEM images of after-shock samples: a. Anhydrite (light contrast grains) and quartz (dark area in between). Shot #1106, 33.8 GPa; b. Anhydrite/gypsum. Shot #1102, 42.1 GPa.

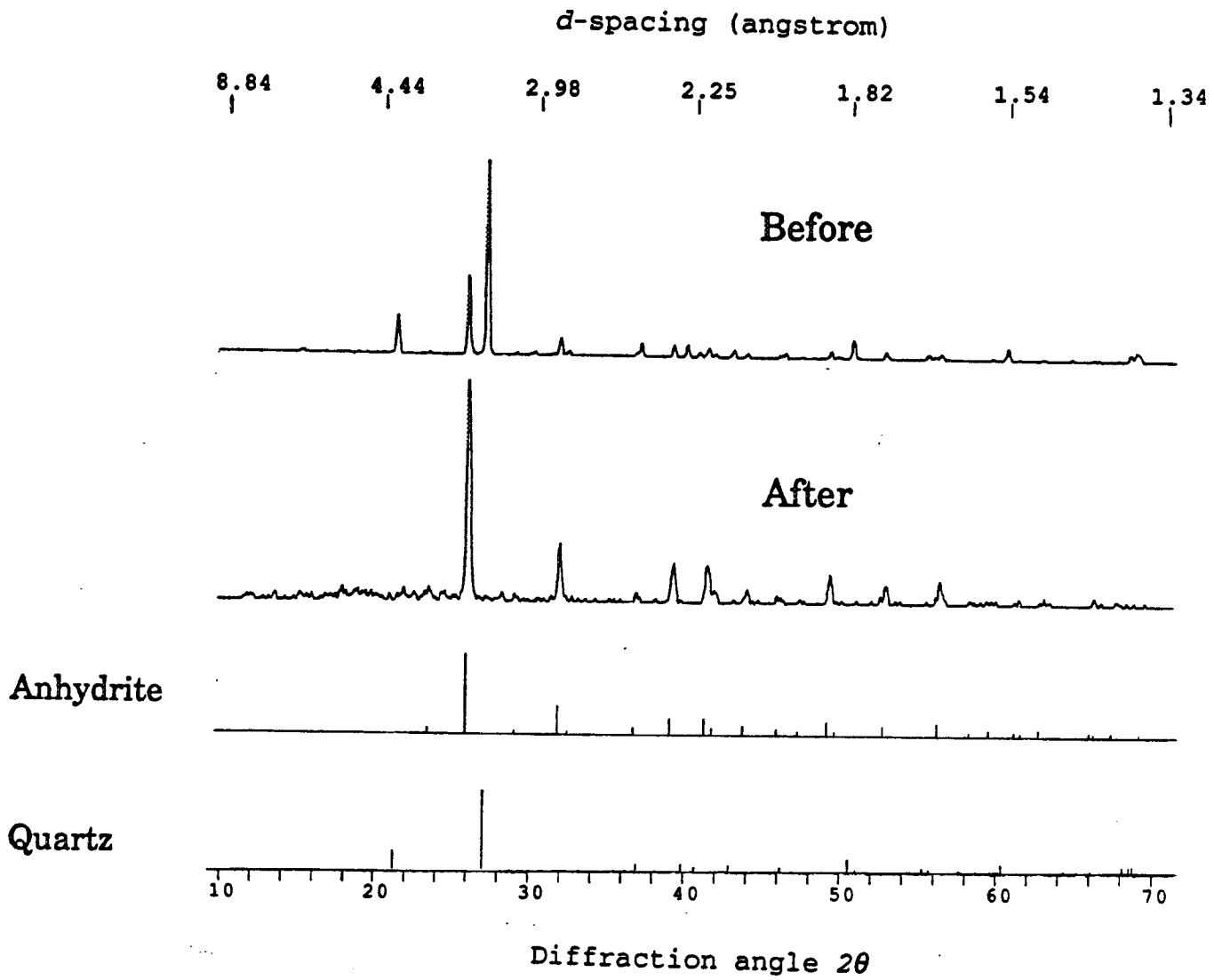


Fig. 2. X-ray diffraction spectra of silica-anhydrite mixture before- and after-shock (Shot #1109, 42.3 GPa). The two spectra at bottom are JCPDS standards for  $\text{CaSO}_4$  and  $\text{SiO}_2$ . Molar ratio of silica to anhydrite is 3:1. Initially crystalline quartz is amorphized in the after-shock material.

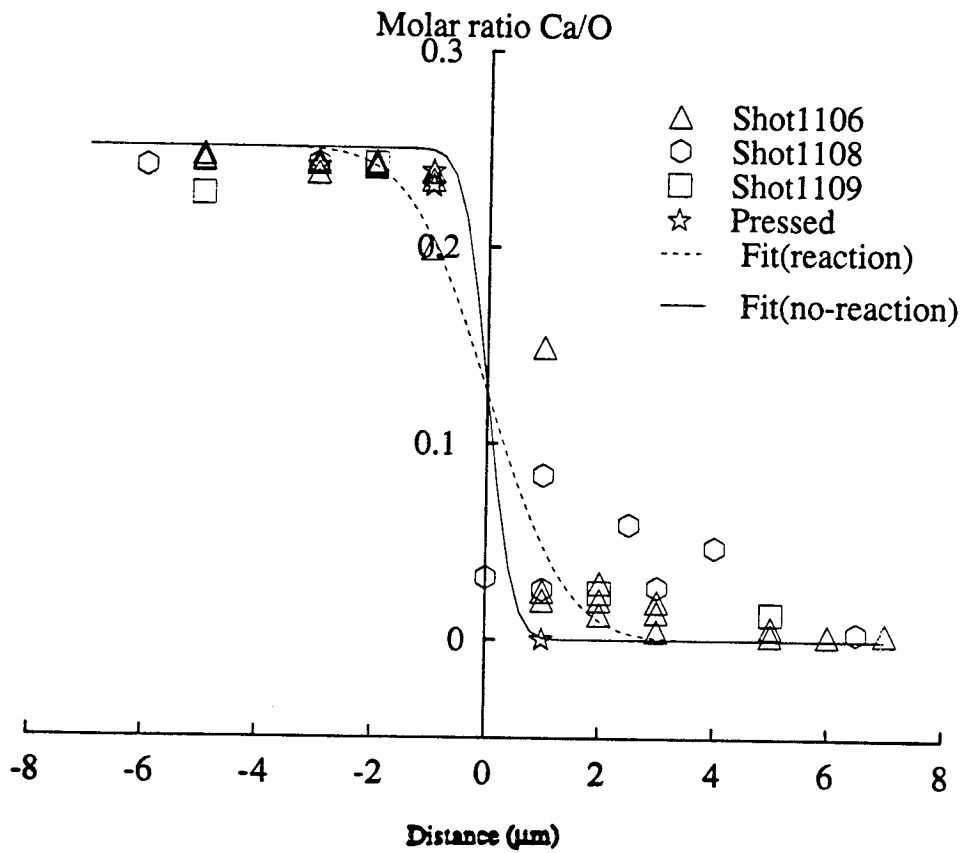


Fig. 3. Atomic ratio of Ca/O profiles of three recovery shots on calcium sulfate and quartz. A cold pressed sample was used to estimate SEM resolution. Theoretical fits are given by Equation 12 with parameters: (1) dashed curve:  $l = 0.53\mu\text{m}$ ,  $L=0$ ; (2) solid curve:  $l = 0.53\mu\text{m}$ ,  $L = 1.5\mu\text{m}$ . The data at  $1\mu\text{m}$  on the dashed curve represent three analyses at different locations near the boundary.

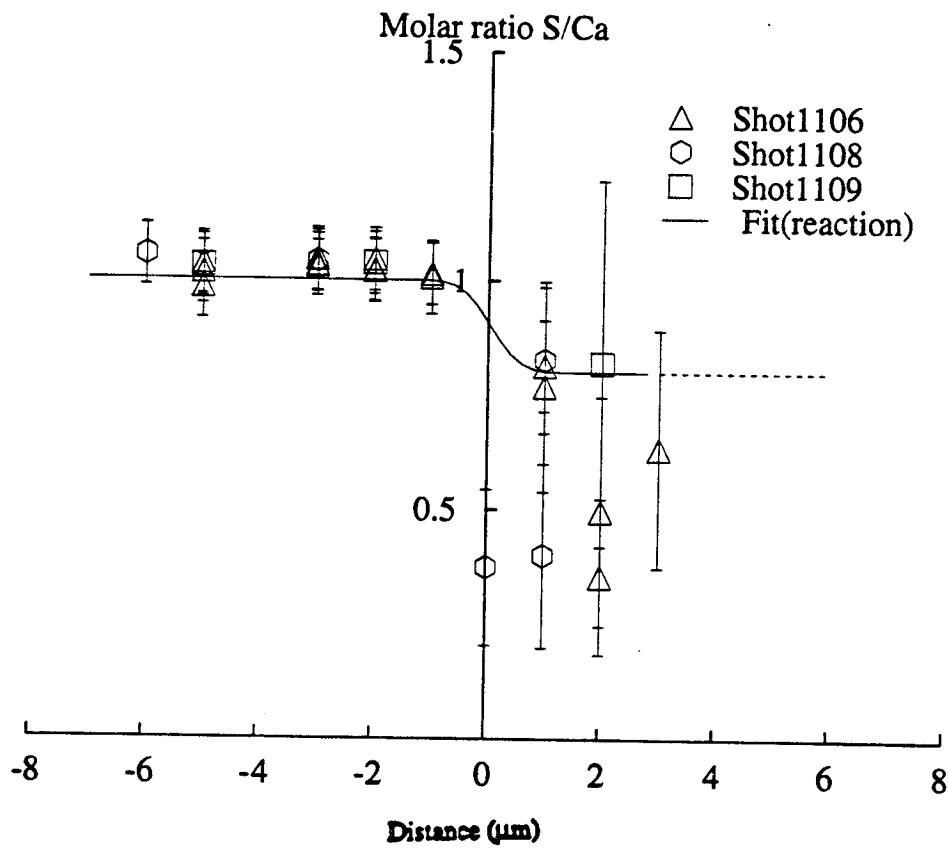


Fig. 4. Atomic ratio of S/Ca profiles of recovery shots on calcium sulfate and quartz. Solid curve is given by Equation 14. Further into  $\text{SiO}_2$ , S/Ca ratio becomes indeterminate and is indicated by the dashed line. Error bars represent SEM analytical uncertainty. Results for other 20 mm shots are similar and not shown.

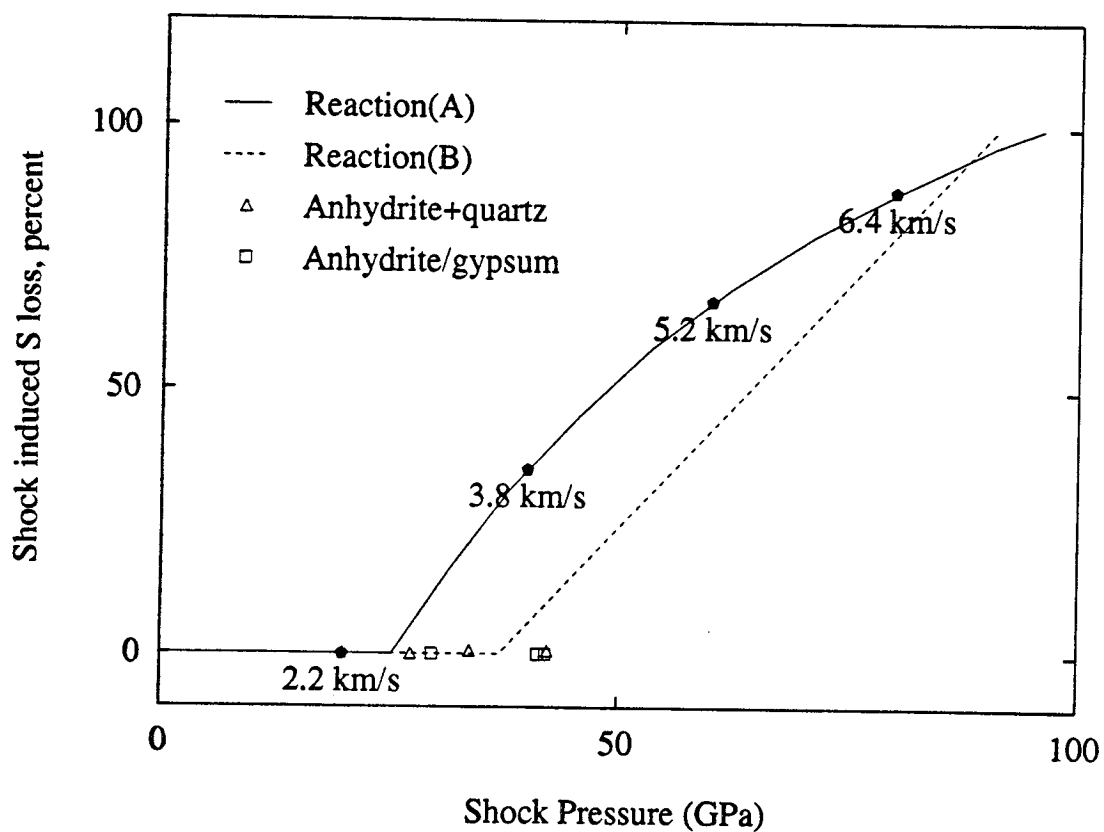


Fig. 5. Degree of devolatilization via reactions (A) and (B) as a function of shock pressure. The curves are calculated using Equations 16-21. Partial pressures of  $O_2$  and  $SO_2/SO_3$  are taken to be 0.2 and  $10^{-4}$  bar respectively in the calculation, which are representative values for normal atmosphere. Impact velocities are indicated for shock pressures of 20, 40, 60 and 80 GPa.

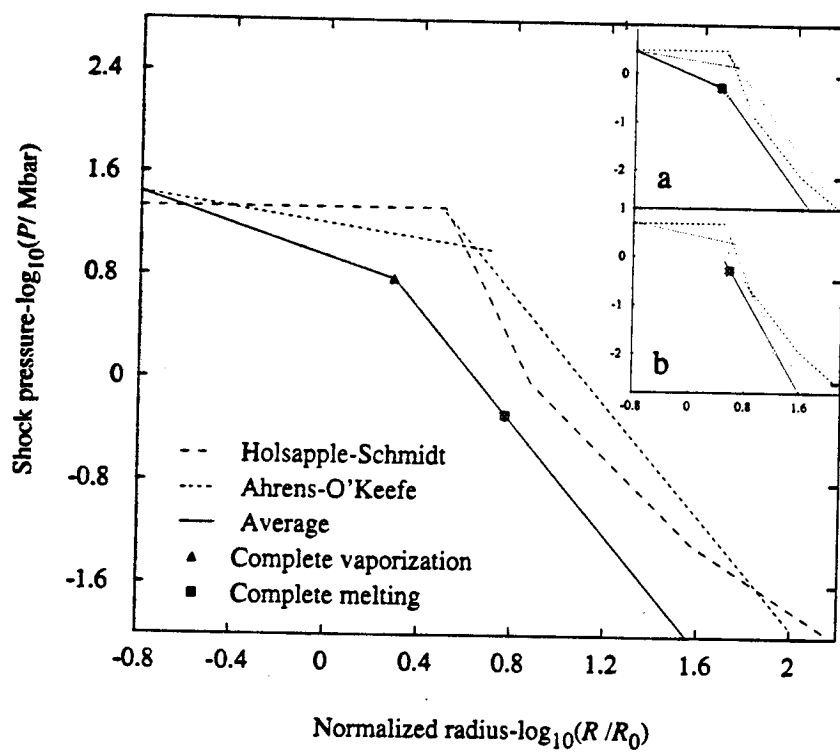


Fig. 6. Shock pressure versus normalized radius at 45 km/s for gabbroic anorthosite impactors. Holsapple-Schmidt scaling relation is also shown for the same impedance-matched center peak pressure. Inset: Pressure attenuation for: a. 15 km/s anorthosite on anorthosite impact; b. 15 km/s iron on anorthosite impact. See text for meaning of "average".

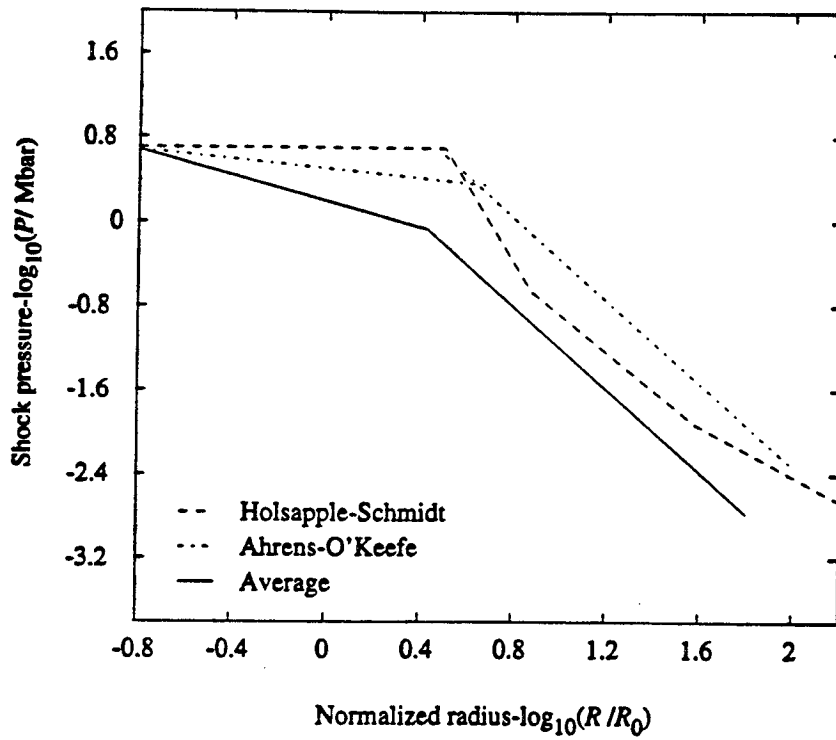


Fig. 7. Shock pressures versus normalized radius for transient Chicxulub crater from an asteroid impact. The bolide and target rock are assumed to have equation of state of gabbroic anorthosite. Bolide initial velocity is 20 km/s,  $R_0=5$  km. Parameters used are listed in Table 5. See text for meaning of "average".